

## Nondestructive interferometric characterization of an optical dipole trap

Plamen G. Petrov,<sup>\*</sup> Daniel Oblak, Carlos L. Garrido Alzar,<sup>†</sup> Niels Kjærgaard, and Eugene S. Polzik  
*QUANTOP, Danish National Research Foundation Centre of Quantum Optics, Niels Bohr Institute, DK-2100 Copenhagen Ø, Denmark*  
 (Received 12 October 2006; published 6 March 2007)

A method for nondestructive characterization of a dipole-trapped atomic sample is presented. It relies on a measurement of the phase shift imposed by cold atoms on an optical pulse that propagates through a free-space Mach-Zehnder interferometer. Using this technique we are able to determine, with very good accuracy, relevant trap parameters such as the atomic sample temperature, trap oscillation frequencies, and loss rates. Another important feature is that our method is faster than conventional absorption or fluorescence techniques, allowing the combination of high-dynamical range measurements and a reduced number of spontaneous emission events per atom.

DOI: [10.1103/PhysRevA.75.033803](https://doi.org/10.1103/PhysRevA.75.033803)

PACS number(s): 42.50.Nn, 03.65.Ta

### I. INTRODUCTION

The first demonstration of optical trapping [1] of laser-cooled atomic samples has paved the way towards nondissipative traps, with long storage times, as well as optical lattices. This relatively long lifetime is associated with low photon-scattering rates in far-off resonant optical traps (FORT), and has made it possible to obtain all-optical Bose-Einstein condensates (BEC) [2,3]. Optical lattices have recently been used to form a storage medium for strontium atoms in an optical atom clock [4], which allows for long interrogation times and higher signal-to-noise ratios. On the other hand, considering the field of quantum information and, in particular, the engineering of quantum states, optical dipole-trapped samples provide a medium with a significant atomic density, a necessary condition for the optimal creation of atomic spin-squeezed states (SSS) [5].

In all of these experiments the characterization of trapped samples is of interest. It has been shown [6] that, in the case of dense atomic samples, noninvasive detection methods are more powerful than the absorption imaging and fluorescence techniques [7]. Nondestructive phase-contrast imaging has already been demonstrated for a sodium BEC in a magnetic trap [8]. The technique of contrast enhancement by implementation of a  $\pi/2$  phase shift between scattered and imaging light is an improved nondestructive dark-ground imaging technique [9], where the off-resonant light is used to image the BEC cloud on a charged-coupled-device (CCD) camera. The phase-contrast method has also been applied in a Rabi oscillation experiment of a rubidium BEC where a superposition between two internal states is created [10]. A spatial heterodyne imaging technique has been used to record the atomic density distribution of a dark-spot magneto-optical-trap (MOT) in the light interference pattern [11]. Recent work introduces the diffraction-contrast imaging as a nondestructive measurement technique [12] of cold atoms.

In this paper we present a method of nondestructive characterization of optically trapped atomic samples, which relies on optical phase-shift measurements in a Mach-Zehnder white-light interferometer, with a sensitivity limited only by the quantum noise of the probe light. The idea behind this interferometric measurement is presented in Ref. [5] as a tool for the creation of squeezed atomic states [13] via a quantum nondemolition (QND) measurement [14]. In the presented work we demonstrate that using relatively low power and large detuning of a probe laser beam, we are able to determine relevant trap parameters as losses, oscillation frequency, and temperature of trapped atoms in a measurement procedure that preserves the atomic sample, as well as the measured parameters and is faster than conventional imaging techniques. Our theoretical and experimental determination of the rate of state depumping and the excitation of atoms in the sample substantiates the nondestructive nature of the measurement. Because of the very high bandwidth achievable by an interferometric measurement, a system similar to ours is projected to be used for nondestructive real-time stabilization of a BEC [15].

The paper is organized as follows. We begin with a short description of the interaction between a polarized light field and an unpolarized atomic sample, followed by the derivation of an equation for the phase shift in our current experimental scheme. Then we proceed with the theoretical analysis of the noise sources in our free-space white-light Mach-Zehnder interferometer. In Sec. III we present our experimental apparatus and the results of our trap characterization.

### II. THEORETICAL DESCRIPTION

#### A. Phase shift of probe light

As it is well known, a two-level unpolarized atomic system influences the phase of a polarized optical (probe) field near a transition between hyperfine ground and excited states. In our case, we consider the alkali  $D$  transition  $J \rightarrow J'$  between states having total electronic angular momenta  $J$  and  $J'$ . The complex index of refraction  $n_\Delta$  imposed on light by a sample of cold multilevel atoms is then given by [16]

<sup>\*</sup>Present address: Department of Physics, Ben Gurion University, Be'er-Sheva 84105, Israel; Electronic address: petrov@bgu.ac.il

<sup>†</sup>Present address: Laboratoire Charles Fabry, CNRS et Université Paris 11, 91403 Orsay, France.

$$n_{\Delta} - 1 = \frac{\lambda^3}{8\pi^2} \sum_{F,F'} N_F S_{JFF'J'} \gamma \frac{\Delta_{FF'} + i\gamma}{\Delta_{FF'}^2 + \gamma^2}, \quad (1)$$

where  $F$  is the total atomic ground-state angular momentum,  $S_{JFF'J'}$  is the dipole transition strength of  $|J, F\rangle \rightarrow |J', F'\rangle$ , and the primed quantum numbers refer to the excited states. We have also introduced  $N_F$  for the atomic density in the level with angular momentum  $F$ ,  $\Delta_{FF'} = \nu - \nu_{FF'}$  for the detuning of the probe light from the  $F \rightarrow F'$  transition, the atomic half width at half maximum (HWHM) linewidth  $\gamma = 2.6$  MHz, and finally, the wavelength  $\lambda$ , assumed to be common for all transitions making up the considered  $D$  line. The real part of the above expression is connected with the phase shift  $\phi_{\Delta} = k_0 l \operatorname{Re}\{n_{\Delta} - 1\}$  imposed on the off-resonant probe light field with wave number  $k_0$  by the interaction with the atomic sample of length  $l$ . The phase shift is proportional to the populations of the atomic levels of concern [5],

$$\phi_{\Delta} = \sum_{F,F'} \phi_F S_{JFF'J'} \frac{\gamma \Delta_{FF'}}{\Delta_{FF'}^2 + \gamma^2}, \quad (2)$$

where  $\phi_F = \frac{\lambda^2 N_F}{2\pi}$  is associated with the phase shift due to atoms on the level with angular momentum  $F$  if the light is near-resonant with  $F \rightarrow F'$ . Equation (2) describes the general case where summation happens over all hyperfine states. In our experiment we use atomic Cs, which has two hyperfine ground states with total angular momentum  $F=3,4$ . Since our probe is blue detuned with respect to the cycling transition  $6S_{1/2}(F=4) \rightarrow 6P_{3/2}(F'=5)$  the phase shift due to atoms on  $F=3$  is negligible and only the atomic population of the  $F=4$  ground hyperfine level contributes to the phase shift in Eq. (2).

### B. Mach-Zehnder interferometer

As mentioned in the previous section, the parameter of interest is the optical phase of the probe light. We choose to monitor the probe-light phase in a separated arms Mach-Zehnder interferometer. One of the arms contains the atomic sample and we refer to it as the probe arm. The other arm is the reference arm. The output of the interferometer is detected by a pulsed balanced homodyne detection scheme. This provides the differential photocurrent  $i_{-} \propto \cos(\tilde{\phi})$  between the detectors in the two output arms. The phase difference along the probe and reference arms is given by  $\tilde{\phi} = 2\pi[\int_{ref} n(L)dL - \int_{probe} n(L)dL]/\lambda$ . The phase can shift due to changes in either the path length or refractive index in one of the arms, or changes in the wavelength of the probe laser. Moreover, in the probe arm the index of refraction can change due to the presence of atoms adding a phase  $\phi_{\Delta}$ , which is the desired imprint of the atomic variable onto the light variable. Therefore, we can write the total phase shift as  $\tilde{\phi} = \phi + \phi_{\Delta}$ , where the last term is the atomic contribution while the first term describes the phase shift due the remaining parameters affecting the optical path length.

To detect the  $\phi_{\Delta}$  one must have controlled influence of the residual phase  $\phi$ . Hence, it is of key importance to identify and minimize the fluctuations of the residual phase that

would otherwise mask the information carried by  $\phi_{\Delta}$ . A comprehensive analysis of the interferometer noise sources was provided in Ref. [5] and here we shall only outline a few main results.

The phase fluctuations due to classical phase noise of the laser vanishes when the interferometer is aligned to the white-light position [5,17]. In this case, the classical amplitude noise of the probe light is canceled by the balanced detection, which corresponds to positioning the interferometer at a half fringe. The only remaining sources of noise are mechanical vibrations that limit the sensitivity of the atomic detection at low frequencies. Nevertheless, with these procedures applied to the system, the interferometric detection is limited by the quantum noise of the probe light, for a wide range of experimental parameters. This shot-noise-limited behavior is documented in Sec. III B

### C. Atomic decoherence and probe excitations

Having addressed the sensitivity of the detection we now turn to an examination of the nondestructive character of the interaction using a convenient parameter for the rate of excitation of atoms caused by the probe light. As before, the fact that the probe is detuned far from the  $F=3 \rightarrow F'=2,3,4$  hyperfine transitions means that the excitations predominantly befall atoms residing in  $F=4$ . These excitations of an atom are characterized by a pulse-integrated probability  $P_{e,4F'}$ ,

$$P_{e,4F'} = \frac{\sigma(\Delta_{4F'})\Phi\tau}{A}, \quad (3)$$

where the absorption cross section for the probe is  $\sigma(\Delta_{4F'}) = (\lambda^2/3\pi)\mathcal{L}(\Delta_{4F'})$ ,  $F'=3,4,5$ ,  $A$  is the cross-sectional area of the probe beam,  $\tau$  is the duration of the probe pulse, and the linewidth functions are given by

$$\mathcal{L}(\Delta_4) = \sum_{F'} S_{4F'} \frac{\gamma^2}{\Delta_{4F'}^2 + \gamma^2}. \quad (4)$$

For typical parameters of our experiment, namely,  $\tau = 2 \mu\text{s}$ , number of photons  $n = \Phi\tau = 1.3 \times 10^6$ , probe beam waist  $w_0 = 20 \mu\text{m}$ , and a blue detuning of  $\Delta_{45'} = 100$  MHz we get a value of  $p_e = 0.034$ .

It should be noted, that with the above choice of probe detuning the excitations primarily populate the  $F'=5$  excited state from which the atoms can only decay back to the  $F=4$  ground state. Calculating the term in Eqs. (3) and (4) which corresponds to excitation to  $F'=4$  one sees that atoms are excited to this level with a probability of only 0.13% per pulse. Hence, while the excitation would destroy the atomic coherences there is only little change in the population distribution among the hyperfine levels. Since, for the results presented here, the atomic sample is initially in a mixed state of all magnetic sublevels the decoherence effect of the probe is not directly relevant.

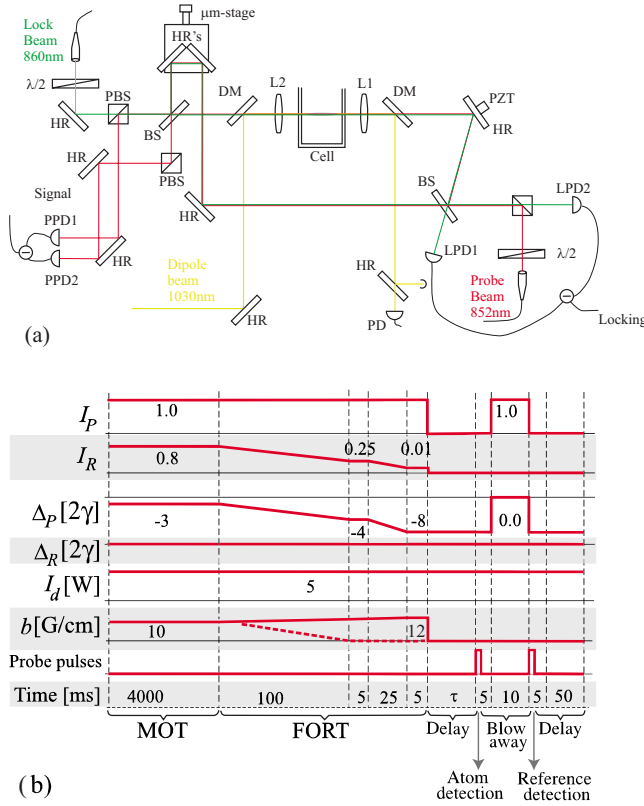


FIG. 1. (Color online). (a) Sketch of the setup of the interferometer with the following elements: BS, 50/50 beam splitter; PBS, polarizing beam splitter; L1 & L2,  $f=100$  mm achromatic lenses; DM, dichroic mirrors (HT @ 852 nm, HR @ 1030 nm); PZT, piezoelectric tube; PPD1 & PPD2, Hamamatsu low noise, high-gain photodiodes for probe detection; LPD1 & LPD2 photodetectors for locking beam detection; and half-wave plates  $\lambda/2$ . (b) Loading sequence of the dipole trap along with detection and reference pulse trains. The probe-pulse duration and repetition rates are specified in the text for the different experiments.

### III. DIPOLE TRAP CHARACTERIZATION

#### A. Atomic sample preparation

The general loading sequence of the dipole trap is shown in Fig. 1(b). Initially, the atomic sample is prepared in a standard six-beam Cs (MOT). The red detuning of the cooling laser is set to  $-6\gamma$ . The number of atoms collected in the MOT varies from  $7.5 \times 10^7$  to  $10^8$  depending on the partial pressure of the Cs vapor. The typical density of the atoms in the MOT is  $1.3 \times 10^9$  atoms/cm<sup>3</sup>.

In the next step, the atoms are further sub-Doppler cooled for 150–200 ms. During this stage the cooling laser detuning is increased to  $-8\gamma$  and simultaneously the intensity of the hyperfine repump light is reduced.

Finally, the cold Cs sample is transferred into a far-off-resonant optical dipole trap (FORT) created by a single light beam focused at the center of the MOT. The dipole trap laser beam is generated by a Yb:YAG laser at a wavelength of 1030 nm. The waist of the trapping beam is estimated to be  $40 \mu\text{m}$ , which along with a power of 3.5 W amounts to a maximum optical potential depth of  $U_{\text{dip}}/k_B = 380 \mu\text{K}$ . The typical density of atoms in the  $F=4$  state is as high as  $8$

$\times 10^{10}$  atoms/cm<sup>3</sup>, which is an increase of almost 62 times compared to the MOT density. The atoms are held in the FORT for variable times from 10 to 1000 ms before being detected with the interferometer.

#### B. Interferometer

The interferometer, as sketched in Fig. 1(a), is in a Mach-Zehnder configuration with free-space propagating beams. Compared with our earlier setup, which employed single-mode fibers [5], this interferometer has significantly lower light losses, but is more susceptible to acoustic and vibrational disturbances. The linearly polarized probe beam hits the interferometer input coupler and splits 50/50 into the reference and the probe arm. The beam in the probe arm is carefully aligned collinearly with the dipole-trapping beam, so that the position of the probe beam waist ( $20 \mu\text{m}$ ) overlaps with the atomic sample. The path length of the reference arm can be coarsely aligned using the mirrors mounted on a translation stage, so that the distances covered by the probe and reference beams, when they are overlapped on the output coupler, are roughly equal. We achieve a maximum fringe visibility of  $\mathcal{V}=98\%$ , which is limited by mode mismatching of the two interferometer arms. The pulsed probe beam is detected with a balanced detection scheme [18] using the low-noise photodiodes PPD1 and PPD2 (Hamamatsu Si PIN S3883). From the integral of the differential photocurrent  $i_-$  over the pulse duration, we extract the pulse area. The mean value gives the phase shift, and the variance gives information about the phase fluctuations.

As in our previous work [5] the Mach-Zehnder interferometer is locked to the interference signal obtained from an auxiliary off-resonant CW laser. The locking beam propagates through the interferometer along the same paths as the probe beam but in the opposite direction and with orthogonal polarization. The wavelength and power of the locking laser are 860 nm and 1 mW, respectively. As discussed in Sec. II B, to suppress the influence of amplitude and phase noise we lock the interferometer to half fringe at the white-light position, corresponding to a nearly zero path-length difference with the help of the procedure described in Ref. [5].

Having implemented all the measures for removing undesirable noise contributions, the fluctuations in our interferometer signal must be due only to the quantum noise of the probe light. As a measure of the instability or noise of the interferometer signal we use the two-point variance  $\sigma^2(\tau_0)$  defined in Ref. [5], which describes the variation of the collected phase shift from a sequence of light pulses with a certain duration  $\tau$  and time separation  $\tau_0$  [22]. In the experiment we send one thousand probe pulses of  $2 \mu\text{s}$  duration with a  $T=6 \mu\text{s}$  repetition period. Then the integrated pulse areas are used to compute the two-point variance,  $\sigma^2(\tau_0)$ .

The quantum shot noise of light will cause the two-point variance to grow proportionally to the probe power. On the other hand, classical noise will result in a quadratic growth of  $\sigma^2(\tau_0)$  with the probe power. To verify the sensitivity of the balanced detection we detect the noise in the amplitude quadrature by splitting the light, from the reference arm only, onto the probe detectors. The fit to the data in Fig. 2 shows

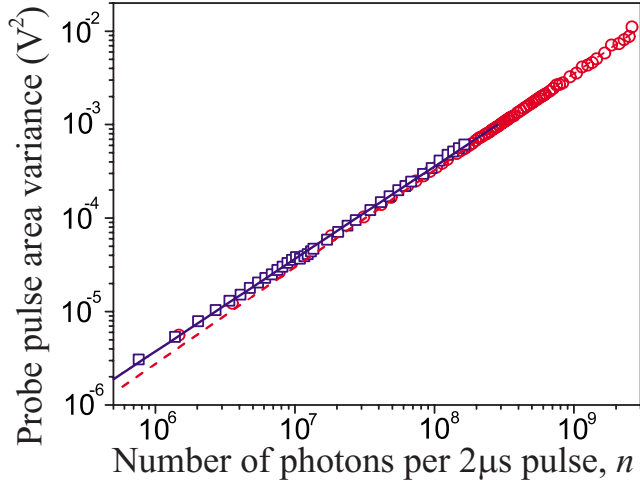


FIG. 2. (Color online). Noise in the amplitude  $x$  ( $\circ$ ) and phase  $y$  ( $\square$ ) quadratures of the probe light. Fits to the data in log-log scale give slopes of  $1.036 \pm 0.008$  [red (dashed)] for the amplitude and  $0.990 \pm 0.005$  [blue (solid)] for the phase quadrature.

that amplitude noise scales linearly with the number of photons in the probe beam, indicating that our balanced detection is shot-noise limited. The detectors remain shot-noise limited on all time scales relevant for the measurements.

Subsequently, we unblock the probe arm, whereby the detection becomes sensitive to phase fluctuations. The result in Fig. 2 shows that the two-point variance scales linearly with the photon number. On this, we conclude that on the  $6 \mu\text{s}$  time scale the detector and interferometer sensitivities are limited only by quantum shot noise for the probe power range from  $0.2\text{--}13 \mu\text{W}$  corresponding to around  $2 \times 10^6\text{--}112 \times 10^6$  photons per  $2 \mu\text{s}$  pulse. When the pulses have a larger temporal separation the interferometer does not remain shot-noise limited for high probe powers. In general the upper power at which the interferometer is shot-noise limited decreases with increasing pulse separation. For measurement on the scale of several ms we find that a probe power of  $150 \text{ nW}$  ensures shot-noise-limited operation and at the same time fulfils the requirement that the detection be nondestructive.

As for the general feasibility of interferometric measurements it has been verified experimentally in a simplified setup [15] that through careful design the acoustic noise can be suppressed to below the shot-noise level on minute-long time scales.

### C. Interferometry with dipole-trapped atoms

In this section we will present the results from the nondestructive characterization of a dipole-trapped atomic sample. Probe light is provided by a grating-stabilized laser diode and detuned by  $100 \text{ MHz}$  from the cycling  $6S_{1/2}(F=4) \rightarrow 6P_{3/2}(F'=5)$  transition in caesium. The probe power is either  $150$  or  $300 \text{ nW}$ . The measurements are done as follows, the dipole trap is loaded using the sequence described in Sec. III A. After a variable storage time delay, but not shorter than  $10 \text{ ms}$ , the atoms in the dipole trap are probed by a train of light pulses with a typical pulse duration of  $2 \mu\text{s}$

and a repetition period of  $6\text{--}100 \mu\text{s}$ , depending on the measurement. The number of pulses is chosen on the purpose of the measurement, but usually varies from  $10$  to  $100$ . After probing the atoms, resonant light from the MOT cooling beams is applied in order to remove the atoms from the probing volume and consecutively, a reference measurement is taken using the same probe-light characteristics. The first measurement collects information about atomic sample, recorded in the light phase, and the second is a reference with no atoms in the probe arm that eliminates the slow drifts of the residual interferometer phase.

In the following we present the results of this measurement method applied to various dynamics of the FORT.

#### 1. Loading and loss dynamics

Here we will apply our nondestructive measurement method to determine the loading and loss parameters of our dipole-trapped atomic sample. A comprehensive analysis of the loading dynamics of a FORT is done by Kuppens *et al.* [7]. The dynamics of the loading process into the  $F=4$  hyperfine ground state are described by the equation:

$$\frac{dN_4}{dt} = R_0 \exp(-\gamma_{\text{MOT}}t) - \Gamma_L N_4 - \beta_L N_4^2, \quad (5)$$

where  $\gamma_{\text{MOT}}$  is the rate at which the MOT loses atoms,  $R_0$  is the loading rate of the dipole trap,  $\Gamma_L$  is the light-assisted loss rate of the FORT,  $\beta_L$  is the light-assisted density-dependent loss rate of the FORT.

When the loading is complete, the MOT trapping fields are switched off and only the FORT potential remains. The evolution of the FORT is then governed by the equation

$$\frac{dN_4}{dt} = -\Gamma N_4 - \beta N_4^2, \quad (6)$$

which contains the light-independent loss coefficients  $\Gamma$  and  $\beta$ . The losses are a result of the natural decay of the dipole trap due to collisions with the background gas particles or with other caesium atoms, and are generally different from the coefficients  $\Gamma_L$  and  $\beta_L$ , which reflect the impact of the MOT light.

For the experimental investigation of the loading of the FORT from the MOT we consider two regimes. In the first *compression* regime the magnetic field is gradually increased from  $10$  to  $12 \text{ G/cm}$  during the loading of the FORT, implying that the density of the MOT increases during the loading. At the end of the loading, the magnetic field is switched off rapidly on a time scale of  $100 \mu\text{s}$  [19]. The detuning of the cooling light at the beginning of loading is  $-6\gamma$ . In the second *molasses* regime the atoms are loaded in the FORT using optical molasses cooling. This means that the magnetic field is switched off gradually during the loading of the FORT [see the dashed line in Fig. 1(b)]. The detuning of MOT light is reduced to  $-13\gamma$ .

In order to determine the loading and loss rates we vary the duration of the loading stage and measure the number of atoms that are loaded into the FORT. The number of atoms as a function of the loading time for two loading schemes are presented in Fig. 3(a). The power of the probe beam is



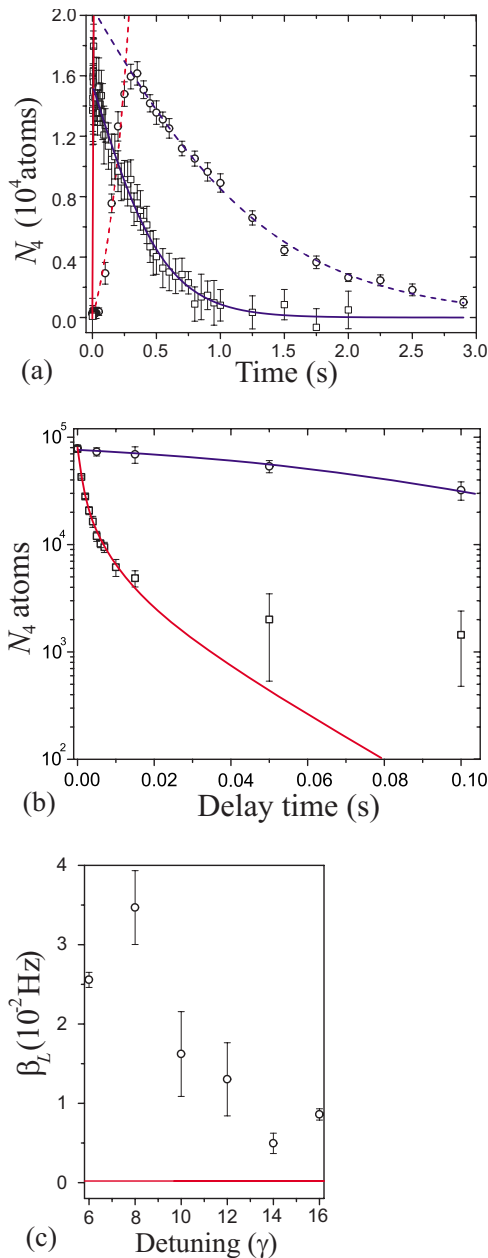


FIG. 3. (Color online). Loading and loss curves of FORT: (a) Number of atoms loaded in the FORT as a function of loading time for the compression ( $\square$ ) and molasses ( $\circ$ ) regimes. The curves are fits to different parts of Eq. (5). (b) Loss curves of FORT. With MOT light on (squares, red curve). Without any MOT light (circles, blue). (c) Light-induced density-dependent losses as a function of light frequency. The line shows the two-body loss level “in the dark.”

$0.3 \mu\text{W}$  and the detuning is set to  $\Delta_{45}=100$  MHz with respect to the cycling  $F=4 \rightarrow F'=5$  transition. The number of atoms is obtained from the mean phase shift of a train of ten pulses with  $2 \mu\text{s}$  duration and a repetition period of  $40 \mu\text{s}$  for the case in Fig. 3(a) (squares) and  $10 \mu\text{s}$  in the case of Fig. 3(a) (circles). Each point in Fig. 3(a) represents an average of 20 experimental runs.

The general solution to Eq. (5) is expressed with Bessel functions, which makes it involved and time consuming to fit

the experimental data on an ordinary PC. To circumvent this issue, we have adopted a method of separating the loading process into two parts: initial loading during which the FORT gains atoms from the MOT, and subsequently the loss of atoms caused by collisions and decay due to cooling light. Thus, for short times we fit to a solution of the differential equation, which includes only the first term on the right-hand side of Eq. (5), and for longer times we fit to a solution of Eq. (5) with only the last two terms.

The values for the loss coefficients obtained from the fits in Fig. 3(a) are compiled in Table I. We see that in the compression regime loading is faster due to the magnetic-field gradient, which keeps the MOT compressed, helping atoms to be transferred to the FORT. However, the density-dependent loss mechanism has a larger effect in compression regime compared to the less-dense molasses regime, where the  $\beta_L$  coefficient is around 30 times lower. The difference in  $\Gamma_L$  between the two regimes is not significant since it does not depend on the atomic density.

Although the above investigation provides a good characterization of the FORT loading, the actual values for the loss coefficients obtained are coupled to the sub-Doppler cooling used to lower the temperature of the atoms. Specifically, the detuning of the light is gradually increased during the loading. To study the light-induced losses independently from the loading process we use the method suggested in Ref. [7]. After storing the atoms in the dipole trap for 10 ms we switch the MOT beams back on with total intensity of the cooling laser of  $4.6 \text{ mW}/\text{cm}^2$ , detuning of  $-16\gamma$ , and repump laser intensity of  $1.1 \text{ mW}/\text{cm}^2$  on resonance. The light is kept on for a varying duration and when it is switched off again the number of atoms remaining in the FORT is measured. Each point in Fig. 3(b) (squares) represents an average value of the number of atoms probed with ten pulses of  $2 \mu\text{s}$  duration and a repetition period of  $40 \mu\text{s}$ . The data is fitted to the solution of Eq. (6) [Fig. 3(b), red curve] and the loss coefficient values obtained from the fit are listed in the third column of Table I. For comparison the losses in the FORT without any MOT light are also measured and plotted in Fig. 3(b) (circles).

The data clearly shows that the FORT undergoes severe losses due to light-assisted collisions, so that the density-dependent losses will prevail over the losses due to background gas collisions. The density-independent loss rate is little affected by the presence of the light. We perform the same measurements at a range of detunings to determine how it affects the light-assisted losses. In Fig. 3(c) we plot the fitted  $\beta_L$  coefficients as a function of the light detuning. As expected we see that the light-assisted losses increase as the detuning is reduced.

## 2. Oscillation frequency

Here we adopt a different measurement technique and demonstrate that using the interferometric measurement we can extract information about important parameters of the FORT in a measurement procedure, which is significantly less time consuming than the conventional methods.

We induce radial oscillation in the FORT by switching the Yb:YAG trapping laser beam off for  $500 \mu\text{s}$  and subse-

TABLE I. Loading and loss parameters of the dipole trap in Hz.

	Compression regime	Molasses regime	Light	No light
$R_0$	$1.34 \times 10^7$	$3.2(6) \times 10^4$		
$\gamma_{MOT}$	831	5		
$\Gamma_L$	3.5	1.2	47(20)	
$\beta_L$	$1.1 \times 10^{-4}$	$3(1) \times 10^{-5}$	$1.1(1) \times 10^{-2}$	
$\Gamma$				21(1)
$\beta$				$2.3(2) \times 10^{-4}$

quently turning it on again. The act of reenforcing the trap potential when the cloud has started to expand will induce a “breathing” oscillation of the radial size of the cloud of atoms, with a frequency that is twice the natural radial oscillation frequency of the trap. These oscillations are exponentially damped due to the anharmonicity of the confining potential. We track the radial breathing mode of the cloud by sending a long pulse train of 100 pulses with  $2 \mu s$  duration,  $100 \mu s$  repetition period, and a power of 150 nW. The result of such a measurement is shown in the inset of Fig. 4. We emphasize that the measurement can be done in a single loading of the FORT and that the atomic sample is not destroyed by the measurement. All in all, the time needed for taking the data is at a maximum of 3 min in the case where we average over 50 cycles. We measured the breathing oscillations for several different values of the dipole beam power. The result is plotted in Fig. 4 and the fitted curve shows that the oscillation frequency follows the anticipated square-root dependence on beam power [20].

The oscillation frequency calculated from the initial estimate of the dipole-beam radius is 2.25 times larger than the measured value. We believe the discrepancy comes from the nonperfect spatial mode of our trapping laser, which can be inferred from the experimentally obtained value for the beam quality factor of  $M^2=1.34$ .

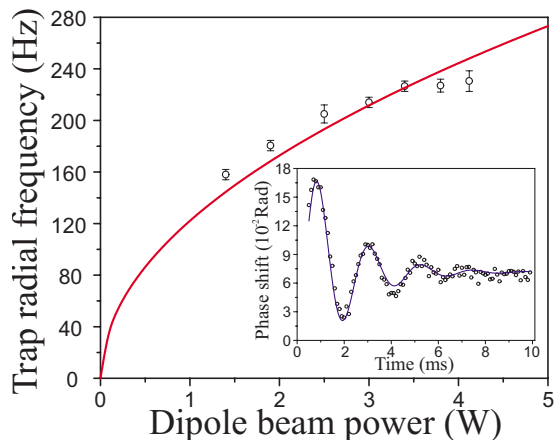


FIG. 4. (Color online). Trap radial oscillation frequency as a function of dipole beam power. The estimated waist of the dipole trap beam from this fit is  $90(1) \mu m$ . The inset: Oscillation in the trap after its revival by switching the dipole trap laser again after  $500 \mu s$  release. The period of the damped oscillations corresponds to an oscillation frequency of  $453(3)$  Hz.

### 3. Temperature

Here we present our measurement of atom temperature using the interferometer phase shift. After storage in the dipole trap the atoms are released by switching off the dipole laser, causing the atomic cloud to expand ballistically in a free fall. During the free expansion the cloud is probed by optical pulses and the measured atomic phase shift is used to determine the fraction of atoms that have left the probe beam volume after a given time. In other words, we can measure the probability  $P(t)$  of an atom initially inside the probe volume, to be outside it after a certain time. The probability  $P(t)$  is found as a convolution of the ballistically expanding density profile and the probing Gaussian light beam. We construct a simple model that describes the evolution of  $P(t)$  as a function of the expansion time and is similar to already known time-of-flight techniques [21]. We derive an approximate expression for the probability function, which has the following form:

$$P(t) = 1 - \frac{w_0^2 + 4\sigma_{r,0}^2}{w_0^2 + 4\sigma_r(t)^2} \exp\left\{-\frac{(gt)^2}{2[w_0^2 + 4\sigma_r(t)^2]}\right\}, \quad (7)$$

where  $w_0=20 \mu m$  is the probe beam waist,  $\sigma_r(t) = \sqrt{\sigma_{r,0}^2 + \sigma_v^2 t^2}$  is the time-dependent radius of an atomic sample with  $g$  the gravitational acceleration,  $\sigma_{r,0} = \sqrt{k_B T / (M \omega_r^2)}$  and  $\sigma_v = \sqrt{k_B T / M}$  being the initial radial extension of the atomic cloud and the initial atom velocity, respectively. Both  $\sigma_{r,0}$  and  $\sigma_v$  depend on the temperature  $T$ , Boltzman’s constant  $k_B$ , the trap radial angular frequency  $\omega_r$ , and  $M$  the atomic mass of  $^{133}Cs$ .

For the measurement the atoms are stored in the dipole trap for 50 ms before being released, after which they are probed by a pulse train with the first pulse arriving just after the atoms are released. The pulse train contains 50 pulses with a duration of  $2 \mu s$ , a repetition period of  $100 \mu s$ , and optical power of 150 nW. The phase shift of each pulse is normalized to the phase shift of the first pulse and the fraction of atoms that have left the probing volume is calculated and plotted in Fig. 5. Hence, each point on the graph in Fig. 5 corresponds to a single pulse and the whole sequence of pulses belongs to a single measurement. Moreover, a single measurement trace represents a complete ballistic expansion of the cloud, free of shot-to-shot fluctuations in the atom number. To correct for any possible decay due to the probe light, we take a reference measurement with the dipole beam

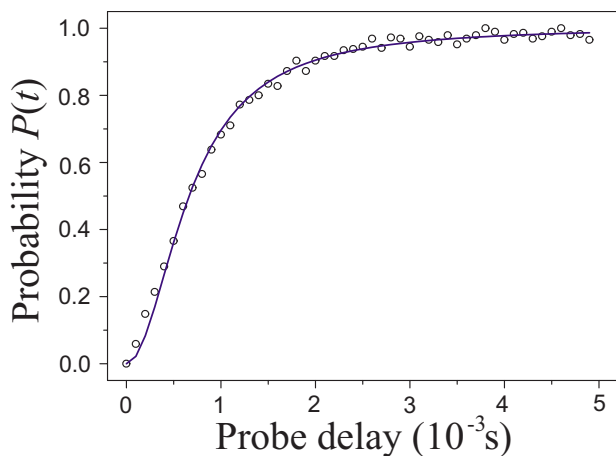


FIG. 5. (Color online). Ballistic expansion of the released atomic cloud probed in a single measurement by a train of 50 pulses, 100  $\mu\text{s}$  apart, with a probe power of 150 nW. The fit to Eq. (7) gives  $T=15(2)$   $\mu\text{K}$ , and  $\nu_r=275(4)$  Hz, respectively, for the temperature and radial oscillation frequency.

on and subtract it from the ballistic data. The estimated relative decay of the detected signal due to probe light depumping is found to be around 3.5%.

The results obtained for the temperature are  $T=15(2)$   $\mu\text{K}$  and oscillation frequency  $\nu_r=275(4)$  Hz. The oscillation frequency is in a reasonable agreement with the previously obtained value of 244 Hz (see Fig. 4) for a power of dipole laser of approximately 4 W.

As a comparison we explore a different measurement procedure, where the evolution of the phase shift during the cloud expansion is compiled from several measurements done at various points of the expansion, similar to what would be the procedure for a destructive measurement. With this method we obtain a temperature estimate of  $T=14.5(2)$   $\mu\text{K}$ , which agrees well with the above value. The radial oscillation frequency estimate of  $\nu_r=259(4)$  Hz fits well with Fig. 4.

As a final verification of the results we directly measure the expansion of the cloud radius using fluorescence imaging on a CCD camera. By this means we get a value for the temperature of 14(2)  $\mu\text{K}$ , which agrees with the interferometric measurements to within 7%.

#### D. Probability of real transitions

Here we want to verify the theoretical estimates of the destructiveness of the measurements due to the absorption of probe light photons, which we in Sec. II C chose to gauge with the parameter  $p_e$ . The absorption of photons from the probe light comes as an inevitable side effect of the dispersive measurement. Since the excitation is followed by spontaneous decay it will heat the sample and decohere the initial atomic state and on a longer time scale depump the  $F=4$  ground level that we are probing.

As the probe is blue detuned by 100 MHz from the  $6S_{1/2}(F=4) \rightarrow 6P_{3/2}(F'=5)$  cycling transition, most excitations will populate the  $F'=5$  excited level from which atoms

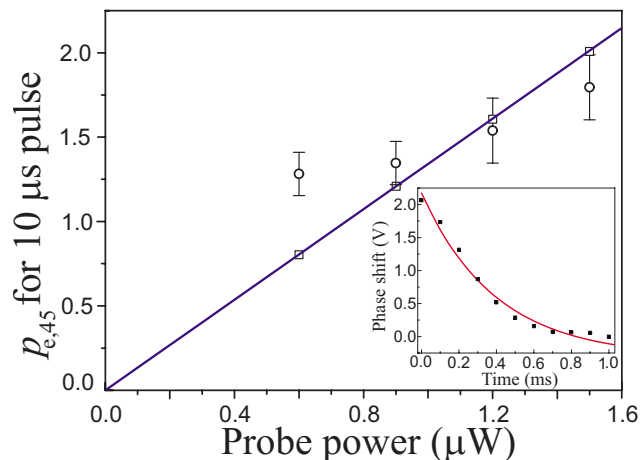


FIG. 6. (Color online). Pulse integrated rate of spontaneous emission. The experimentally obtained value for the  $p_e$  parameter as a function of the probe power for a 10- $\mu\text{s}$ -long probe pulse: values of  $p_e$  for different powers obtained from the fit of the phase-shift decay ( $\circ$ ), theoretically calculated values for a probe beam waist radius of 21.2  $\mu\text{m}$  ( $\square$ ), and a linear fit to the data (solid line). The inset shows the raw data for probe power of 1.2  $\mu\text{W}$ .

can only decay back to the  $F=4$  ground level. The experimental method for estimating  $p_e$ , however, relies on the small chance of exciting atoms to the  $F'=4$  excited state whereupon the atoms may decay to either the  $F=3$  or  $F=4$  ground levels. Hence, the excitation to the  $F'=4$  level will cause a reduction of population in the  $F=4$  ground state that we can observe as a reduction of the phase shift. Since the depumping parameter is proportional to the number of photons, we monitor the decay of the interferometer phase shift as a function of the probe power. The direct experimental parameter is the characteristic time constant of the decay that we expect to decrease linearly with increasing probe power.

In the experiment we send a long pulse train consisting of 40 pulses of 10  $\mu\text{s}$  duration and 100  $\mu\text{s}$  repetition period through the atomic sample along with a reference pulse train. Each pulse in the train causes a small amount of depumping, which causes a smaller phase shift of the subsequent pulse in the train. An example of a measurement trace for a probe power of 1.2  $\mu\text{W}$  is shown in the inset of Fig. 6. Altogether, the measurement is done at four different power levels of the 100 MHz blue-detuned probe beam.

The decay is modeled by a set of rate equations that take into account the two ground levels, the  $F'=4$  and  $F'=5$  excited levels, and two optical fields, namely, the probe and residual hyperfine repump fields. For a given probe power the value of  $p_e$  is obtained by fitting the decay of the phase shift to the expression obtained from the rate equations. The values of the depumping parameter are plotted against the probe power and fitted to a straight line as shown in Fig. 6. We can theoretically calculate  $p_e$  using Eqs. (3) and (4) and if we use a probe waist radius of 21.2  $\mu\text{m}$  [23] the theoretical estimates coincide with the experimental fit. We see that for very low probe powers the pulse-integrated probability of spontaneous emission per atom is less than one. The lowest power used in our characterization measurements is 150 nW for a pulse duration of 2  $\mu\text{s}$ . This would mean that the lowest

photon-scattering probability per atom is of the order of  $p_e = 0.038$ . Hence, in terms of the depumping of the  $F=4$  level and the loss of atoms due to heating we can regard the measurement to be nondestructive.

#### IV. CONCLUSION

In this paper we have demonstrated a method for the non-destructive characterization of a dipole-trapped atomic sample using a shot-noise-limited free-space white-light Mach-Zehnder interferometer.

The radial oscillation frequencies and temperature measurements were done in a single loading run, thus enabling us for fast characterization of the atomic sample. The temperature measurement in both single and multiple runs agrees with the one obtained by fluorescence detection using a CCD camera. Furthermore, an estimation of the nondestructive character of the measurement has shown a pulse-

integrated probability of real transition for an atom to be as low as 0.038.

The real-time monitoring of the phase shift in a Mach-Zehnder interferometer allows for the fast and nondestructive characterization of atomic samples. The method is applied to a dipole-trapped atomic sample but with the same success it can be expanded to Bose-Einstein condensates, where the optical density is much higher and the absorption imaging does not give the necessary contrast [8]. Moreover, our pulsed detection scheme allows for microsecond time scale monitoring of processes and phenomena taking place in an atomic cloud with a few thousand atoms, which in other cases as absorption or fluorescence imaging are not visible due to the limited measurement bandwidth.

#### ACKNOWLEDGMENTS

This research has been supported by the Danish National Research Foundation and by European network CAUAC via Contract No. HPRN-CT-2000-00165.

- 
- [1] S. Chu, J. E. Bjorkholm, A. Ashkin, and A. Cable, *Phys. Rev. Lett.* **57**, 314 (1986).
  - [2] M. Barrett, J. Sauer, and M. S. Chapman, *Phys. Rev. Lett.* **87**, 010404 (2001).
  - [3] T. Weber, J. Herbig, M. Mark, H.-C. Nägerl, and R. Grimm, *Science* **299**, 233 (2003).
  - [4] M. Takamoto, F.-L. Hong, R. Higashi, and H. Katori, *Nature (London)* **435**, 321 (2005).
  - [5] D. Oblak, P. G. Petrov, C. L. Garrido Alzar, W. Tittel, A. K. Vershovski, J. K. Mikkelsen, J. L. Sørensen, and E. S. Polzik, *Phys. Rev. A* **71**, 043807 (2005).
  - [6] J. E. Lye, J. J. Hope, and J. D. Close, *Phys. Rev. A* **67**, 043609 (2003).
  - [7] S. J. M. Kuppens, K. L. Corwin, K. W. Miller, T. E. Chupp, and C. E. Wieman, *Phys. Rev. A* **62**, 013406 (2000).
  - [8] M. R. Andrews, M. O. Mewes, N. J. van Druten, D. S. Durfee, D. M. Kurn, and W. Ketterle, *Science* **273**, 84 (1996).
  - [9] M. Andrews, C. Townsend, H.-J. Meisner, D. Durfee, D. Kurn, and W. Ketterle, *Science* **275**, 637 (1997).
  - [10] M. R. Matthews, B. P. Anderson, P. C. Haljan, D. S. Hall, M. J. Holland, J. E. Williams, C. E. Wieman, and E. A. Cornell, *Phys. Rev. Lett.* **83**, 3358 (1999).
  - [11] S. Kadlecek, J. Sebby, R. Newell, and T. Walker, *Opt. Lett.* **26**, 137 (2001).
  - [12] L. D. Turner, K. F. E. M. Domen, and R. E. Scholten, *Phys. Rev. A* **72**, 031403(R) (2005).
  - [13] M. Kitagawa and M. Ueda, *Phys. Rev. A* **47**, 5138 (1993).
  - [14] A. Kuzmich, N. P. Bigelow, and L. Mandel, *Europhys. Lett.* **42**, 481 (1998).
  - [15] C. Figl, L. Longchambon, M. Jeppesen, M. Kruger, H. A. Bachor, N. P. Robbins, and J. D. Close, *Appl. Opt.* **45**, 3415 (2006).
  - [16] I. I. Sobelman, *Atomic Spectra and Radiative Transitions* 2nd ed. (Springer, Berlin, 1992).
  - [17] A. Dandridge, *J. Lightwave Technol.* **3**, 514 (1983).
  - [18] H. Hansen, T. Aichele, C. Hettich, P. Lodahl, A. I. Lvovsky, J. Mlynek, and S. Schiller, *Opt. Lett.* **26**, 1714 (2001).
  - [19] C. L. Garrido Alzar, P. G. Petrov, D. Oblak, J. H. Müller, and E. S. Polzik, *physics/0701251*.
  - [20] D. Boiron, A. Michaud, J. M. Fournier, L. Simard, M. Sprenger, G. Grynberg, and C. Salomon, *Phys. Rev. A* **57**, R4106 (1998).
  - [21] D. Weiss, E. Riis, J. Shevy, P. Ungar, and S. Chu, *J. Opt. Soc. Am. B* **6**, 2072 (1989).
  - [22] The time separation  $\tau_0$  is an integer multiple of the repetition period  $T$ .
  - [23] The value agrees with the measured one of 20  $\mu\text{m}$ .